Research Square

Preprints are preliminary reports that have not undergone peer review.
They should not be considered conclusive, used to inform clinical practice,
or referenced by the media as validated information.

Surface Albedo as an Early Indicator of Landscape Change in the Amrapali Coal Mine Overburden of Eastern India

Sonu Choudhary
ICFRE - Institute of Forest Productivity
Surojit Konar
ICFRE - Institute of Forest Productivity
Yogheshwar Mishra
ICFRE - Institute of Forest Productivity
Sharad Tiwari
tiwaris@icfre.org

ICFRE - Institute of Forest Productivity

Research Article

Keywords: Coal mine overburden, Ecological restoration, Land Surface Temperature, Mutli-temporal-framework, NDVI, Surface albedo

Posted Date: November 24th, 2026

DOI: https://doi.org/10.21203/rs.3.rs-11688461/v1

License: This work is licensed under a Creative Commons Attribution 4.0 International License.
Read Full License

Additional Declarations: No competing interests reported.

Surface Albedo as an Early Indicator of Landscape Change in the Amrapali Coal Mine Overburden of Eastern India

Sonu Choudhary[1], Surojit Konar[1], Yogheswar Mishra[1], Sharad Tiwari[1*]

[1]ICFRE - Institute of Forest Productivity, Ranchi, Jharkhand - 835303, INDIA

Sonu Choudhary: sonuc3107@gmail.com; ORCID: *https://orcid.org/0009-0007-4092-9294*

Surojit Konar: surjitkonar1@gmail.com; ORCID: *https://orcid.org/0009-0006-7090-3143*

Yogeshwar Mishra: mishray631@gmail.com; ORCID: *https://orcid.org/0000-0003-0003-5118*

*Sharad Tiwari: tiwaris@icfre.org; ORCID: *https://orcid.org/0000-0003-4902-8349*

(Corresponding Author: Sharad Tiwari email: tiwaris@icfre.org, sharadtiwari8@gmail.com , Cell: +919431766404)

Abstract

Monitoring coal-mine rehabilitation primarily relies on single vegetation indices, which reflect greenness but overlook surface transitions that precede vegetation growth, and are rarely integrated into a reproducible spatio-temporal workflow. Surface albedo is a promising yet underutilized metric for early-stage reclamation, but integrated multi-indicator assessments remain sparse. This study addresses this gap for the Amrapali opencast coal-mine overburden in Chatra, Jharkhand, establishing a pre-restoration baseline (2013–2026). Annual composites of surface albedo, land surface temperature (LST) and NDVI were derived from Landsat imagery across a 10 km buffer, and land use/land cover (LULC) change was quantified (2015–2025). Trends were assessed with OLS regression, the Mann–Kendall test and Sen's slope, and relationships with Pearson and Spearman correlations. Surface albedo showed a significant declining trend (Mann–Kendall $p = 0.004$; Sen's slope = -0.00137 yr^{-1}; $R^2 = 0.60$), the clearest signal of landscape change, consistent with progressive darkening of the stabilizing overburden. NDVI showed no significant trend but high variability (CV = 13.4%), and LST remained stable despite an approximately 3.7-fold mine expansion. A significant inverse NDVI–LST relationship (Spearman $\rho = -0.55$, $p = 0.043$) confirmed vegetation cooling, whereas weak albedo–LST and NDVI–albedo associations indicate that surface material changes, not canopy greenness, governed the albedo decline. LULC analysis documented contraction of open land (~−39%) and vegetation (~−16%) alongside mine, built-up and agricultural expansion. By fusing albedo, LST, NDVI and LULC in a spatially-explicit, multi-temporal framework built on openly available data, this study identifies albedo as a sensitive early-stage indicator and contributes a transparent, transferable geospatial workflow and baseline for evaluating future restoration.

Keywords: Coal mine overburden, Ecological restoration, Land Surface Temperature, Mutli-temporal-framework, NDVI, Surface albedo

1. Introduction

Coal mining is among the most ecologically disruptive forms of land use, generating large volumes of overburden material resulting in a bare, denuded surface (Frouz 2021; Haigh et al. 2020). Opencast mineral extraction destroys the land surface by excavating massive open pits causing altered local water regimes, habitat fragmentation and land degradation that obstruct natural vegetation growth (Ekka et al. 2023; Szarek-Łukaszewska 2009). By disrupting complex natural ecosystems, mining fundamentally alters the land surface energy balance (Deng et al. 2015). Previous research across major coal producing regions has established that these disturbances affect the land surface energy balance, significantly altering vegetation cover NDVI, the surface's reflective behaviour, and its thermal response (Firozjaei 2021). Specifically, the systematic degradation of vegetation correlates with a prominent rise in Land Surface Temperature (LST) and changes in surface albedo, creating localized "heat islands" and destabilizing microclimatic conditions (Kandulna et al. 2025). Understanding these dynamics is essential to assess the environmental footprint of mining and develop restoration strategies for mined out areas amidst climate change (Chen et al. 2025).

There are many published studies that have established that surface albedo is a key parameter in land surface energy balance, microclimate regulation, and climate studies, and is effectively retrievable from satellite observations (Zhang et al. 2022; Shuai et al., 2020). In the coupled soil-vegetation-atmosphere system, albedo controls the partitioning of absorbed radiation into sensible and latent heat fluxes, thereby influencing surface temperature and ecosystem processes (McGregor 2024). Land surface temperature, in turn, is a sensitive indicator of the surface thermal environment and is strongly modulated by land cover (Zhou & wang 2010). Both albedo and evapotranspiration generally exhibit negative correlations with LST (Trilica et al. 2017) and increasing vegetation cover has repeatedly been shown to reduce surface temperature, creating localized cooling effects that help regulate microclimate (Millward et al. 2014). At broader scales, vegetation cover produces competing biophysical effects on surface temperature-cooling through enhanced energy dissipation and evapotranspiration but warming through reduced albedo with the net effect across temperate and tropical environments generally favour cooling (Best et al. 2023).

Disturbed mining landscapes with bright, bare overburden, sparse vegetation, and built-up surfaces present a heterogeneous mosaic of albedo and thermal conditions (Bi et al. 2025). This spatial complexity makes an integrated analysis of vegetation, albedo, and LST especially informative for assessing surface change, as it captures the physical and thermal transitions that a single index might miss (Wu et al. 2022). Despite extensive research on coal-mine rehabilitation globally, comparatively few studies particularly in the Indian context integrate vegetation, surface albedo, and land surface temperature into a single multi-year, spatially explicit assessment of an active overburden landscape. The present study addresses this gap for the Amrapali coal-mine overburden in Chatra, Jharkhand. Using time-series (2013-2026) annual remote sensing derived NDVI, surface albedo, LST, and land use/land cover (LULC) data, the objectives of this study are: (i) to characterize the temporal trends of surface albedo, LST, and NDVI ; (ii) to examine the inter-relationships among these biophysical variables; (iii) to quantify decadal LULC change across the landscape; and (iv) to establish a quantitative pre-restoration biophysical baseline against which the effects of the rehabilitation interventions through afforestation can be evaluated in future polygon specific monitoring.

2. Methodology

This section outlines the overall methodological framework adopted in the present study, comprising study area buffering, data acquisition and pre-processing, and the analytical procedures used to assess vegetation dynamics over the mine overburden and its buffer.

2.1 Amrapali mining area buffer

We drew a 10 km buffer radius around the Amrapali coal mine over burden site (Fig. 1), to capture both the direct mine footprint and the surrounding zone of ecological influence, including peripheral forest fragmentation, hydrological regimes, and rural settlements (Tang & Werner 2023). Within this buffer area, we quantified temporal changes in LULC classes and correlated these changes with NDVI, LST, and albedo.

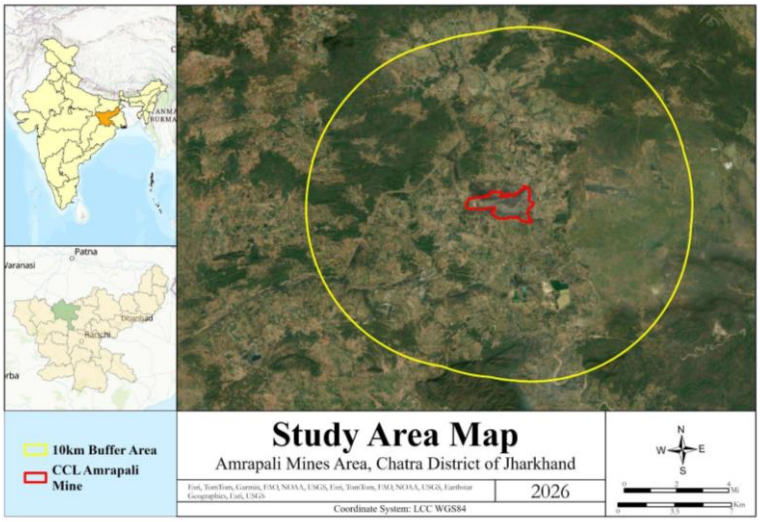

Fig. 1. Location of the Amrapali open-cast coal mine study area, Chatra district, Jharkhand, India. The buffer area considered in this study is delineated by the yellow circle, and the overburden site is demarcated by the red polygon.

2.2 Data Acquisition and Preprocessing

We obtained Level-1 Terrain-Corrected (L1TP) Landsat 8 Operational Land Imager (OLI) and Thermal Infrared Sensor (TIRS) data from the USGS EarthExplorer platform as the primary data source for this study. We selected the pre-monsoon period (March–May 2013–2026) to minimise cloud cover interference and capture maximum thermal and vegetation stress conditions (Mansingh et al. 2026). We converted raw Digital Numbers (DN) to physical units, transforming optical bands into Top-of-Atmosphere (TOA) planetary reflectance and Band 10 thermal infrared data into brightness temperature (T_B) (Prasad et al. 2025). We then applied the FLAASH module to correct sub-pixel atmospheric attenuation and isolate accurate surface reflectance values (Gong & Wu 2014).

2.3 Extraction of Biophysical Parameters

We derived biophysical parameters including Normalised Difference Vegetation Index (NDVI), Surface Albedo and Land Surface Temperature (LST) for the 10 km buffer area across the Amrapali coal mine overburden landscape for 2013-2026 period. These are detailed in subsections given below:

2.3.1 Normalised Difference Vegetation Index (NDVI)

We calculated the Normalised Difference Vegetation Index (NDVI) for the mining buffer area using ArcGIS 10.8 Raster calculator. The index utilises the surface reflectance of the Near infrared (NIR) Band 5 and Red (RED) Band 4 spectral bands:

NDVI = (NIR) - (RED)/(NIR) + (RED)

2.3.2 Land Surface Temperature (LST) Estimation

We derived the Land Surface Temperature (LST) from TIRS Band 10 data. First, we isolated the fractional vegetation cover P_v from the retrieved NDVI thresholds (NDVI_min, NDVI_max). We then used this parameter to calculate the Land Surface Emissivity ϵ using the threshold method:

$$\epsilon = \epsilon_v P_v + \epsilon_s (1 - P_v) + C$$

Where ϵ_v (0.985) and ϵ_s (0.960) represent the emissivity values of vegetation and soil, respectively, and C= 0.004 accounts for surface roughness.

Finally, we compounded LST by correcting the brightness temperature (T_B) for emissivity using the single channel algorithm:

$$LST = \frac{T_B}{1 + \left(\frac{\lambda \cdot T_B}{\rho}\right) \ln(\epsilon)}$$

where,

λ is the effective wavelength of Band 10 (10.895μm) and ρ (constant) $h.c/\sigma$ $(1.438 \times 10^{-2} mK)$.

2.3.3 Surface Albedo

Albedo determines how much of the incoming shortwave radiation a surface reflects rather than absorbs, so a shift in albedo registers early in the processes that shape the surface energy balance (Gottschalk et al. 2026). We calculated Surface albedo (α) to evaluate the radiative balance transitions caused by land clearance and mining activities. We applied the empirical weight coefficients defined by Liang (2001) were applied to integrate the visible, near-infrared, and shortwave infrared bands within the GIS environment:

$$\alpha = 0.356\,(b_2) + 0.130\,(b_3) + 0.373(b_4) + 0.085\,(b_5) + 0.072\,(b_6) - 0.018$$

where b_n corresponds to the surface reflectance values of the respective Landsat 8 bands.

3. Land Use Land Class (LULC) map

We generated a Land Use Land Cover (LULC) map using the Supervised Classification method by applying the Maximum Likelihood algorithm to the optical bands (Patil et al. 2012). We established five distinct land classes: Active Mining Pits, Vegetation, Water Bodies, Agricultural land, NTPC area, Open Land and Built-up Land. Training samples were selected uniformly across the study area based on Area of Interest (AOI) polygons verified via high resolution

historical imagery from Google Earth Pro (Maxwell et al. 2019). To validate classification performance, an independent set of validation pixels was used to construct a confusion matrix, yielding the Overall Accuracy (OA) and the Kappa coefficient (κ) (Foody 2020).

2.4 Statistical Analysis

We conducted all statistical analyses on the annual, scene-wide values of NDVI, surface albedo and LST derived for the 10 km buffer over the 2013–2026 period (n = 14 years), treating each year as a single observation in the time series. Prior to trend testing, we summarised each indicator using descriptive statistics (annual mean and standard deviation) and expressed relative dispersion as the coefficient of variation (CV = $\sigma/\mu \times 100$).

We tested each indicator for monotonic change over the study period using three methods. First, we fitted ordinary least squares (OLS) linear regression of the annual value against year, reporting the slope, coefficient of determination (R^2) and the associated p-value of the slope as a parametric measure of linear trend. Because a series of only 14 points may deviate from normality and is sensitive to outliers, we employed non-parametric Mann–Kendall test (Mann 1945; Kendall 1975), which evaluates the direction and significance of a monotonic trend without assuming a distribution; we calculated the standardised statistic (Z) and its p-value. Finally, we quantified the magnitude of change using the Theil–Sen slope estimator (Theil 1950; Sen 1968). We did not impose a before/after split around the December 2024 intervention, as it falls at the end of the series and whole-scene statistics cannot resolve it.

To examine the inter-relationships among the biophysical indicators, we computed pairwise correlations between NDVI, albedo and LST using both the parametric Pearson product-moment coefficient (r; Pearson 1895) and the non-parametric Spearman rank correlation coefficient (ρ; Spearman 1904). We report both because Pearson assesses linear association whereas Spearman captures monotonic association and is more robust to non-linearity and the small sample size; associations were considered statistically significant at $p < 0.05$.

For the supervised LULC classification, we assessed classification performance against an independent set of validation pixels using a confusion (error) matrix, from which we derived the Overall Accuracy (OA) and the Kappa coefficient (κ) (Foody 2020). Throughout, we adopted a significance threshold of $\alpha = 0.05$ and denote significance levels as *** $p < 0.001$, ** $p < 0.01$, * $p < 0.05$, and ns = not significant. All trend and correlation computations were performed in a Python (SciPy/statsmodels and pymannkendall) environment, and the confusion-matrix accuracy assessment was carried out within the GIS environment.

3. Results

This study characterises the long term spatio-temporal pattern of biophysical surface parameters-Normalised Difference Vegetation Index (NDVI), Surface Albedo and Land Surface Temperature (LST) together with Land Use / Land Cover (LULC) change, across the Amrapali coal mine overburden landscape in Jharkhand over 2013-2026. While interpreting the results, it is important to note that in 2018 a small part~1 hectare of the mining overburden site was revegetated. We also note that a Miyawaki plantation was established on the site in December 2024; but we deliberately treat it as the

endpoint and motivation for future monitoring rather than as a causal factor. Therefore, the 2013-2026 trends reported here provide the reference state against which the plantation's later ecological effects can be evaluated.

3.1 Descriptive Time-Series Statistics

Annual mean (μ) and standard deviation (σ) of the three continuous indicators derived from the source imagery is given shown Fig.2. Over the record, NDVI ranged 0.145-0.221, surface albedo 0.077-0.098, and LST 35.1-44.1 °C.

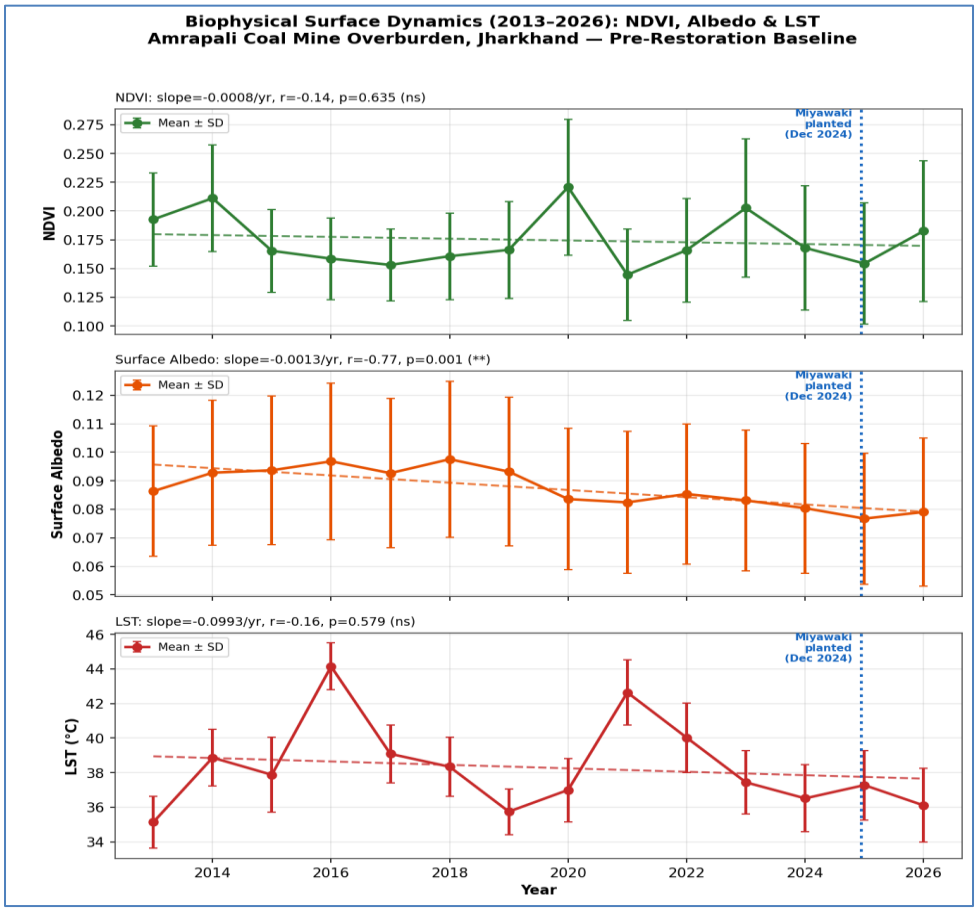

Fig. 2. Temporal trends of NDVI, Surface albedo and LST (2013-2026) with linear trend lines (dashed) and ±1 SD error bars. The dotted blue line marks the December 2024 Miyawaki planting-the start of the monitoring period, not a modelled breakpoint.

3.2 Trend analysis and statistical validation

To test monotonic change across the studied period, we applied three complementary methods: ordinary least squares (OLS) linear regression, the non-parametric Mann-Kendall trend test, and Sen's slope estimator (Table 1). We did not impose an artificial before/after split, because the only intervention (Dec 2024) lies at the series end and whole-scene statistics cannot resolve it. Significance: *** $p<0.001$, ** $p<0.01$, * $p<0.05$, ns = not significant.

Table 1. Full-series trend statistics for each biophysical indicator

Variable	OLS slope/yr (p)	R^2	Mann-Kendall Z (p)	Sen slope/yr	CV %
NDVI	-0.00078 (0.635ns)	0.019	0.00 (1.000)	-0.00009	13.4
Surface Albedo	-0.00127 (0.001**)	0.597	-2.85 (0.004)	-0.00137	7.9
LST (°C)	-0.09926 (0.579ns)	0.026	-0.77 (0.443)	-0.15142	6.7

3.2.1 Surface Albedo- significant decline

Surface albedo is the only indicator with a statistically significant monotonic trend. OLS regression yields a negative slope of -0.00127 yr^{-1} ($r = -0.77$, $R^2 = 0.60$, $p = 0.001$), confirmed by the Mann–Kendall test ($Z = -2.85$, $p = 0.004$) and a Sen's slope of -0.00137 yr^{-1}. Fig.2 shows that the mean albedo declined from 0.098 (2018) toward 0.077 (2025).

3.2.2 NDVI-no significant trend, high variability

We found no significant monotonic trend in NDVI (OLS $p = 0.635$; Mann-Kendall $p = 1.000$) and the highest inter-annual variability of the three indicators (CV = 13.4%). NDVI reached its peak greenness (0.221) in 2020 and the minimum (0.145) in 2021. This fluctuation, with no sustained directional change, reflects rainfall and phenology driven variability typical of a disturbed, partially vegetated mining landscape and establishes the variable vegetation baseline against which we will assess the plantation.

3.2.3 Land Surface Temperature- stable

We found no significant trend in LST (OLS $p = 0.579$; Mann-Kendall $p = 0.443$). Annual means oscillated between 35.1°C (2013) and 44.1°C (2016) around a baseline mean of 38.3°C. Differences in acquisition date and season, rather than persistent surface change, drove much of this year-to-year variation, and the absence of a warming trend across an actively expanding mine remains a notable feature of the baseline.

3.2.4 Inter-Variable Relationships

Pairwise correlation tests the expected biophysical coupling among the indicators. NDVI and LST show a negative association, and Spearman's rank test confirms that this relationship is statistically significant (Spearman $\rho = -0.55$, $p = 0.043$; Pearson $r = -0.43$, $p = 0.12$), reflecting the anticipated vegetation-cooling signal in which greener surfaces tend to have lower surface temperature (Fig. 3). The Albedo-LST ($r = 0.32$) and NDVI-Albedo ($r = -0.13$) associations are weaker and non-significant, suggesting that changes in surface material drive the albedo decline more than canopy greenness alone.

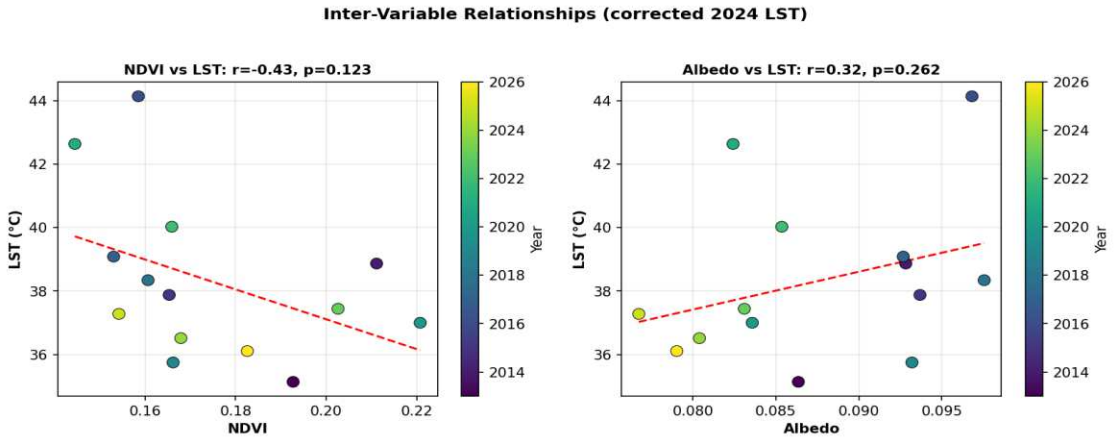

Fig. 3. Scatter relationships of NDVI-LST and Albedo-LST, colour coded by year, with linear fits. Inter-variable relationships between land surface temperature (LST) and the two biophysical indicators over the study period (2013–2026). Left panel: NDVI versus LST; right panel: surface albedo versus LST. Each point represents one annual scene-wide value, coloured by year (colour bar). The red dashed line denotes the ordinary least squares regression fit. Pearson correlation coefficients and their p-values are shown above each panel: NDVI–LST ($r = -0.43$, $p = 0.123$) and albedo–LST ($r = 0.32$, $p = 0.262$), neither being statistically significant at $\alpha = 0.05$.

3.3 Spatial pattern and distribution

Figures 3-6 show the spatial distribution of each variable across the Amrapali mine and its surrounding area. These maps support the temporal statistics by revealing the geographic organisation of surface change that scene-wide averages alone cannot capture. Each annual panel uses an independent value range; therefore, spatial interpretation focuses on within-scene patterns and the per-year value ranges reported in the legends rather than on direct colour comparison between panels.

3.4 Land Use / Land Cover

Fig. 4 shows the progressive expansion of the active mine footprint (grey) across 2015, 2020 and 2025, along with the contraction of open land and natural vegetation and the intensification of built-up and agricultural classes in the later period. The spatial growth of the mine class visually mirrors its near tripling in area reported in Section 6, and mining and built-up surfaces increasingly encroach on previously vegetated and open land areas around the central and southern parts of the scene.

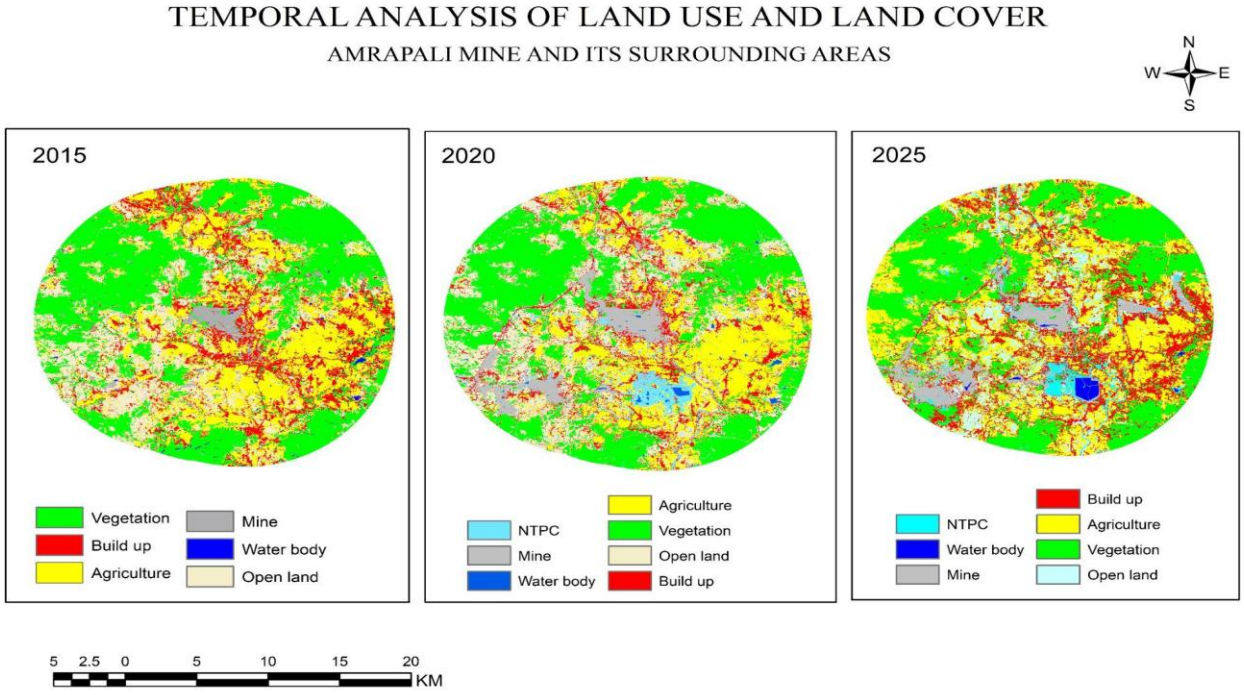

Fig. 4. Land Use Land Class map of the 10km buffer area around the mining overburden landscape for the periods 2015,2020 and 2025.

3.5 Surface Albedo

Figure S1 shows high-albedo surfaces (warm colours) concentrated over bare overburden, built-up, and exposed areas, and low-albedo surfaces (cool colours) over vegetated terrain. Consistent with the significant declining trend identified by the Mann-Kendall test (Section 3.1), the upper bound of the per-panel albedo range generally decreases over the record. Earlier years show higher maxima (e.g. ~0.25 in the mid-2010s) than the most recent years (~0.20), indicating progressive surface darkening as bare spoil gives way to soil development and vegetation cover across the wider landscape.

3.6 Normalized Difference Vegetation Index (NDVI)

Figure S2 shows generally high greenness (lighter tones) over the vegetated hill areas and lower values over the mine, built-up, and water surfaces. Across the record, the spatial pattern remains broadly stable without a consistent directional shift, and the per-panel value ranges fluctuate rather than showing a spatially consistent trend, in line with the absence of a significant monotonic NDVI trend and the high inter-annual variability reported in Section 3.2.

3.7 Land Surface Temperature (LST)

Figure S3 shows warm surfaces (red/orange) over the mine, built-up, and exposed areas and cooler surfaces (blue) over vegetated terrain in each year. This spatial pattern expresses the significant negative NDVI–LST association reported in Section 4, in which greener surfaces correspond to lower surface temperatures. The per-panel temperature ranges vary across years in line with acquisition date and seasonal differences (Limitations), consistent with the absence of a significant monotonic LST trend.

3.8 Land Use / Land Cover Change (2015–2025)

Over the 2015–2025 period, the landscape of the study area underwent substantial conversion, while the total classified area remained effectively constant (~43,000 ha). The most pronounced changes were a contraction of open land and

vegetation, offset by the expansion of built-up, agricultural and mining classes (Fig. 5, Fig. 6). It can be seen from the Fig. 6, that within the study area there is a major contraction in the Open land (-3,477 ha, -39.0%) and vegetation (-2,550 ha, -15.9%), while built-up areas increased by 2,284 ha (+34.8%) and agriculture by 1,878 ha (+17.8%). This conversion of natural and open surfaces to built-up, agricultural and mining land is consistent with the significant landscape-scale decline in surface albedo reported in Section 3.1.

Open land experienced the largest absolute and relative decline, shrinking from 8,908 ha to 5,431 ha a net loss of 3,477 ha, equivalent to a 39.0% reduction and falling from 20.7% to 12.6% of the total area. Vegetation showed the second-largest loss, decreasing from 16,014 ha to 13,464 ha (a net 2,550 ha, or 15.9%), so that its share of the landscape declined from 37.2% to 31.3%; despite this reduction it remained the single most extensive class throughout the period. Water bodies contracted only marginally, from 351 ha to 315 ha (−36 ha, −10.3%), leaving their areal share essentially unchanged (~0.8%).

Taken together, the reciprocal loss of open land and vegetation (a combined ~6,027 ha) against the growth of built-up, agricultural and mining land indicates a decade of intensifying anthropogenic pressure, in which natural and unused surfaces were progressively converted to settlement, cultivation and active mining.

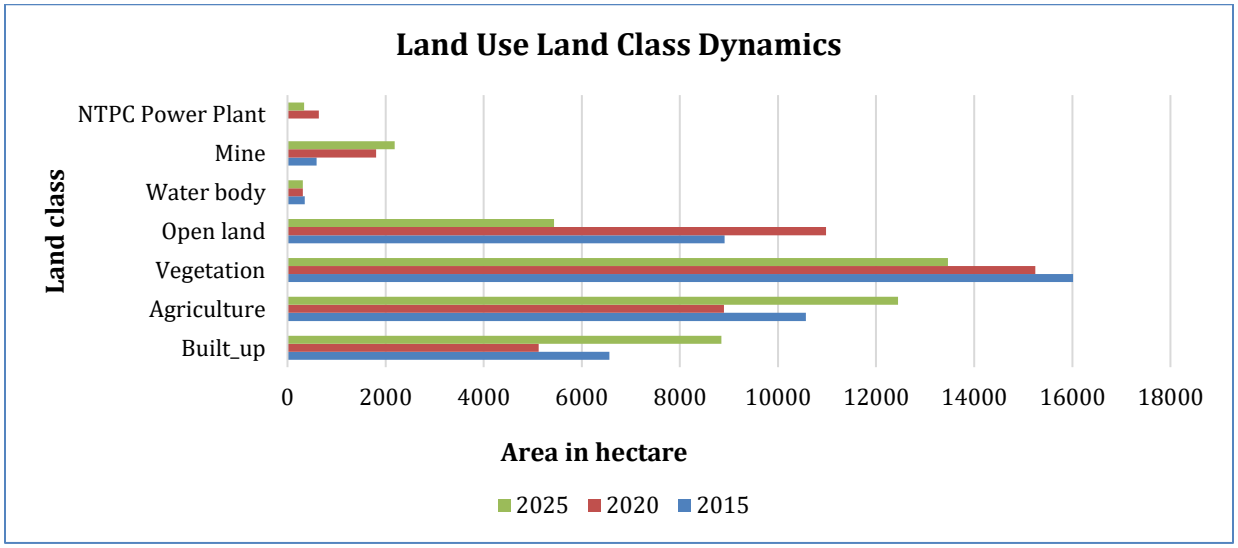

Fig.5. Class-wise distribution of Land Use / Land Cover (LULC) area (in hectares) across the study area for the years 2015, 2020 and 2025. Grouped bars compare the extent of each of the seven LULC classes at the three time points, illustrating the progressive contraction of open land and vegetation alongside the expansion of built-up, agricultural and mining classes.

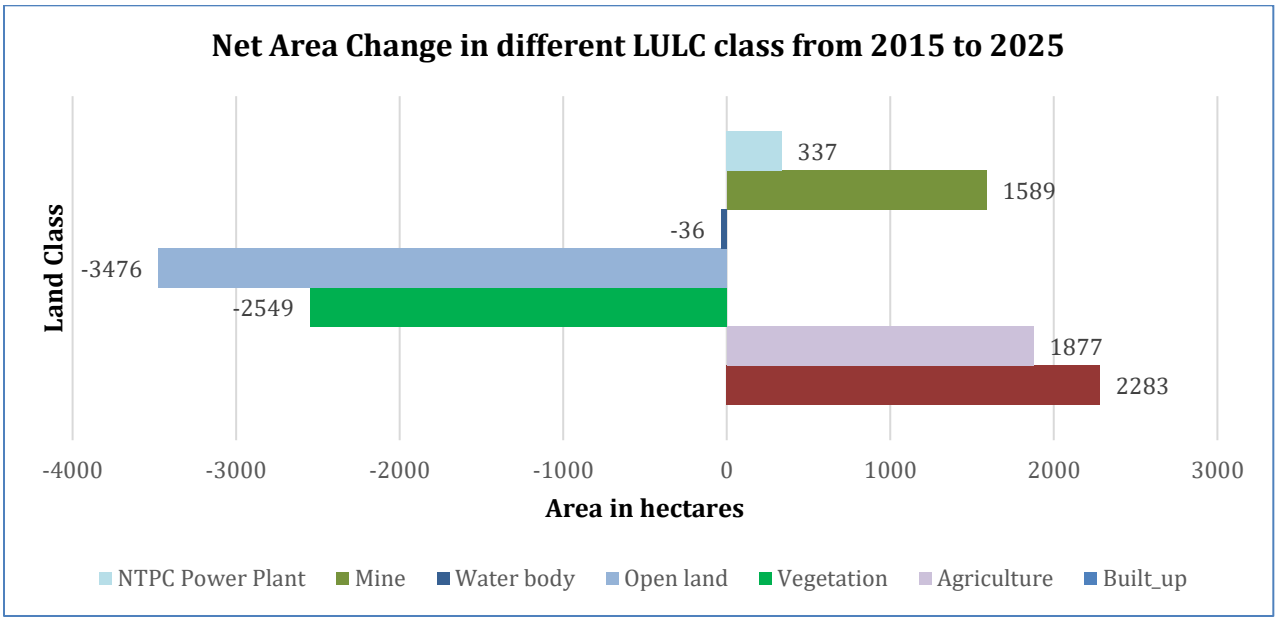

Fig. 6. Net change in Land Use / Land Cover (LULC) area (in hectares) for each class over the period 2015–2025. Positive (green) bars denote net areal gain and negative (red) bars net loss; values represent the difference between the 2025 and 2015 class areas, highlighting the largest reductions in open land (−3,477 ha) and vegetation (−2,550 ha) against the largest gains in built-up (+2,284 ha) and mine (+1,590 ha) classes.

Overall, for the 2013-2026 baseline data, the dominant biophysical signal was a significant landscape scale decline in surface albedo (Mann-Kendall, $p < 0.01$), consistent with progressive darkening and partial revegetation of the overburden surface. NDVI showed no directional trend but high interannual variability, defining a fluctuating vegetation baseline governed largely by climate and phenology. LST likewise showed no significant trend, only a slight, non-significant cooling tendency, despite continued mine expansion, although the expected NDVI–LST cooling relationship was statistically significant under the rank-based Spearman test ($\rho \approx -0.55$, $p < 0.05$). LULC dynamics documented substantial change: major losses of open land and vegetation alongside expansion of mining, agriculture and built-up classes. Together, these results establish a pre-restoration reference state in which albedo, rather than NDVI or LST, carries the clearest directional signal of surface transformation.

4. Discussion

The study identified surface albedo as the most sensitive and statistically significant indicator of overburden surface change. The progressive decline in albedo is consistent with progressive darkening of the overburden surface as bare spoil is replaced by soil development and incremental vegetation cover across the wider landscape over the baseline period (Vicentini et al. 2020). The non-significant albedo-NDVI association indicates that the darkening was primarily due to the changed surface properties rather than by a measurable increase in green vegetation alone. It implies that in the early, pre-canopy stages of overburden stabilisation, surface reflectance responds to substrate maturation before vegetation indices register a directional signal, making albedo a leading rather than a lagging indicator of surface recovery (Tahooni et al. 2024). One important note worth mentioning here is that although a small conventional plantation was established on approximately 1-2 ha of the overburden in 2018-19 broadly coinciding with the onset of the post 2018 albedo decline. This patch is negligible relative to the large study area and cannot, on its own, account for the landscape scale trend; this

reinforces the interpretation that the albedo signal reflects broader surface material maturation rather than any single localised planting.

Contrary to the expectations this study found absence of net warming despite significant expansion (~ 267%) in mining area and open land contraction ~39%. This contrasts with most of the studies that report vegetation loss elevates surface temperature (Makarieva et al. 2022, Waseem & Khayyam 2019). This could be attributed to the fact that the study area covers a 10 km buffer dominated by vegetation, agriculture and open land rather than focusing only on the overburdened part. So, the scene-wide means dilute the strong but spatially confined thermal signal of the excavation itself (Arvidson et al. 2026). Additionally, the significant inverse NDVI-LST relationship endorsed the vegetation cooling mechanism remains functional at the landscape scale (Weng et al. 2004; Sun et al. 2025). Further, despite concurrent declining albedo, the nonsignificant warming suggests that compensating processes enhanced evapotranspiration from maturing surfaces, soil moisture and surface roughness changes, and the partitioning of additional absorbed energy into latent rather than sensible heat may have offset the radiative effect (Burakowski et al. 2018; Rotenberg & Yakir 2010).This phenomenon is in agreement with the physical framework established by Feldman et al. (2023), who demonstrated that when soil moisture is sufficient, the expected warming from low albedo surfaces becomes statistically nonsignificant. Another study by Dominguez-Haydar et al. (2019) corroborates our observations, which identified a clear transition where mature reclaimed surfaces act as thermal sinks, mitigating the high temperature anomalies typically associated with active mining pits. Together, these processes suggest that the structural and hydrological maturation of the site has created a microclimate capable of neutralizing increased radiative forcing. (Zhang et. al. 2023)

The findings revealed that NDVI exhibited no directional trend but the highest inter annual variability of the three indicators (CV = 13.4%), with greenness peaking in 2020 and troughing in 2021. Such fluctuations are typical of a partially vegetated, disturbance prone landscape in which annual vegetation signals do not reflect permanent ecological shifts, but are sensitive to pre monsoon rainfall, phenological timing and data acquisition date (Mutti et al. 2020). The area consists of a patchwork of active mining, reclaimed plots, and vegetation residue, the pixel integrated NDVI is subject to nonlinear mixing; this mosaic introduces spatial autocorrelation issues (Frazier & Kedron 2017). In these heterogeneous pixels, even minor shifts in the data acquisition date can lead to significant phenological offsets, because different vegetation patches require different time intervals to reach peak greenness (Senf et al. 2017). The lack of a directional trend in NDVI, may also highlight the saturation or sensitivity limits of the index in disturbed soils. In a sparse vegetation landscape dominated by bright bare spoil and exposed soil, NDVI is known to be sensitive to soil background reflectance (Montandon & Small 2008), which can inflate inter-annual noise and partially mask weak vegetation trends (Yengoh et. al. 2015). Such settings necessitate employing soil-adjusted indices such as Soil Adjusted Vegetation Index (SAVI) or Modified Soil Adjusted Vegetation Index (MSAVI) or moisture resilient metrics to decouple the reclamation progress from the stochasticity of the monsoon cycle (Yang et al. 2025). These indices may resolve early vegetation establishment across the mining-agriculture-forest mosaic more sensitively than NDVI alone (O'Donnell et. al. 2024). NDVI-albedo dissociation supports the argument that, during the pre-canopy phase of recovery, vegetation indices alone provide an incomplete picture of surface change and are significant when interpreted jointly with radiative and thermal indicators precisely the integrated approach adopted in this study (Wang et. al. 2025b).

Overall, these findings suggest that single period NDVI data are insufficient indicators of reclamation success in disturbance prone mining landscapes and calls for two major complementary refinements in monitoring approach (O'Donnell et. al. 2024). The first concerns temporal sampling. NDVI responds strongly to pre-monsoon rainfall and acquisition timing (Deka et al. 2019) and therefore risks conflating ephemeral growth pulses or dry-spell signals with genuine successional trends (Li et al. 2024). This can result in false readings of degradation or recovery that reflect image acquisition date rather than real change. To address this, employing phenological normalization techniques, such as constructing peak greenness composites from multi temporal stacks (Snyder et al. 2019) or calculating Rain Use Efficiency (RUE) to account for precipitation driven pulses (John et al. 2016) can isolate the genuine maturation signal from monsoon driven noise (Ratul et al. 2014).

The second concerns spectral formulation. In a heterogeneous mosaic of bare overburden, reclaimed plots, and remnant vegetation, NDVI's sensitivity to soil background means that changes in soil moisture or surface roughness can be misread as changes in greenness. Soil-adjusted indices such as (SAVI) or Modified Soil Adjusted Vegetation Signal (MSAVI) or spectral unmixing approaches would allow the green vegetation fraction to be isolated from the underlying soil matrix, enabling more sensitive resolution of early vegetation establishment across the mining-agriculture-forest mosaic than NDVI alone permits (Yang et al. 2025).

Together, these refinements coupled with the integrated radiative thermal framework adopted in this study offer a sound basis for distinguishing genuine reclamation trajectories from the inherent stochasticity of disturbed, dryland mining landscapes. The findings carry direct implications for monitoring overburden rehabilitation initiatives (Shen et. al. 2017). Because the albedo declines here tracked surface material maturation rather than greening, it offers means of distinguishing genuine substrate stabilisation from transient, rainfall driven vegetation flushes that inflate NDVI without durable surface change. The thermal stability documented under active expansion suggests, encouragingly, that maintaining and expanding vegetated and agricultural cover within the mine's zone of influence can buffer the wider landscape against thermal degradation (Poole & Berman 2001) even as excavation continues; a result of practical relevance to mine closure planning and to restoration designed around landscape connectivity. The integrated, multi-indicator baseline itself provides the quantitative reference state against which the ecological trajectories of both the 2018-19 conventional plantation and the December 2024 Miyawaki plantation, and of future interventions, can be objectively evaluated.

Beyond its ecological findings, this study contributes to Earth science informatics by demonstrating an integrated, reproducible workflow for spatio-temporal analysis of post-mining landscapes from earth-observation data. Rather than relying on a single spectral index, it fuses four remotely-sensed information layers surface albedo, land surface temperature, NDVI, and land use/land cover within one spatially-explicit, multi-temporal framework, coupled with a formal analytical layer combining parametric and non-parametric trend detection (OLS, Mann–Kendall, Sen's slope) and correlation analysis (Pearson, Spearman). Its principal informatics contribution is to show that structured integration of complementary biophysical layers resolves early-stage surface transitions here, albedo-detected overburden stabilization—that conventional single-index approaches fail to capture, thereby increasing the information content of change detection in spectrally heterogeneous terrain. Because the workflow is built entirely on openly available Landsat data and standard geospatial and statistical operations, it is transparent, reproducible, and transferable to other overburden

and degraded-land settings. The resulting quantitative geospatial baseline and repeatable analytical pipeline provide a foundation for operational, polygon-specific monitoring of restoration interventions, illustrating how disciplined integration of routine earth-observation datasets can extend their diagnostic reach.

Nevertheless, some limitations of the present study need to be acknowledged here. The analysis considered scene wide averaging over a 10 km buffer, which dilutes spatially confined signals, so the absence of a net LST trend should not be read as the absence of localised thermal intensification over the pit itself. NDVI's sensitivity to soil background in bright overburden settings may understate or add noise to the vegetation signal. LST retrieval depends on an NDVI-threshold emissivity scheme (Wang et al. 2025a), so the vegetation and thermal estimates are not fully independent, and emissivity assumptions over heterogeneous spoil surfaces carry uncertainty (Hulley et. al. 2012). Another factor that merits caution refers to the two localised afforestation efforts that fall within the study area-a small conventional plantation of roughly 1-2 ha in 2018-19 and the Miyawaki plantation established in December 2024. Yet both are a negligible relative to the 10 km buffer and cannot be resolved as causal factors by these whole scene statistics; the baseline is therefore effectively pre-intervention at the landscape scale, with the December 2024 planting falling at the very end of the record. Finally, the moderate spatial resolution of Landsat (30 m optical; 100 m resampled thermal) limits the detection of fine scale, polygon specific restoration responses (Ončillová et. al. 2022).

While this study has its limitations, it offers a better insight into mining ecology. The study suggests that post mining recovery is more than just developing green area coverage. (Zine et. al. 2024) By showing that changes in surface reflection appear long before new growth shows up on a satellite, the study shifts how we define early recovery. This is crucial, because conventional vegetation indices focused on reclamation assessment may systematically overlook the substrate development phase (Stokes et al. 2014), as soil background reflectance often masks subtle biological crusting or stabilization (Escribano et al. 2010). By quantifying the thermal buffering provided by retained vegetation at the landscape scale, it links biophysical monitoring to the ecological function of cooling and microclimate regulation that supports habitat suitability for rehabilitating local biodiversity. (Huang et. al. 2022). The methodology provides a low cost, satellite-based protocol framework that can be easily applied across similar landscapes for establishing ecological insights. (Pettorelli et. al. 2014)

5. Conclusion

This study established a pre-restoration biophysical baseline for the Amrapali coal-mine overburden in Chatra, Jharkhand, from a 13-year Landsat record (2013–2026) across a 10 km buffer. Surface albedo declined significantly over the period, making it the clearest directional signal of surface transformation and consistent with progressive darkening and partial revegetation of the overburden. NDVI showed no directional trend but marked interannual variability, defining a fluctuating vegetation baseline driven by climate and phenology. LST likewise showed no significant trend, only a slight non-significant cooling tendency despite continued mine expansion, although its inverse relationship with NDVI was confirmed by rank-based correlation. LULC analysis showed that this apparent stability masked substantial compositional change: open land and vegetation declined markedly while mining, agriculture and built-up classes expanded.

Acknowledgement:

The authors gratefully acknowledge the Director, ICFRE–Institute of Forest Productivity, Ranchi, for administrative support and providing the necessary facilities to carry out this work.

Code and Data Availability:

Data availability: The satellite data analysed in this study are publicly available. Landsat 8 Operational Land Imager (OLI) and Thermal Infrared Sensor (TIRS) Collection 2 Level-1 scenes for 2013–2026 were obtained from the U.S. Geological Survey (USGS) EarthExplorer portal (https://earthexplorer.usgs.gov/), dataset "Landsat 8-9 OLI/TIRS C2 L1" (Earth Resources Observation and Science (EROS) Center, Landsat 8-9 Operational Land Imager and Thermal Infrared Sensor Collection 2 Level-1 [dataset], U.S. Geological Survey, https://doi.org/10.5066/P975CC9B). High-resolution reference imagery used to verify LULC training and validation samples was accessed through Google Earth Pro (https://earth.google.com/). Code availability: The Python code implementing the descriptive, trend (OLS, Mann–Kendall, Sen's slope) and correlation (Pearson, Spearman) analyses is available from the corresponding author on reasonable request.

Conflict of Interest: Authors declare no conflict of interest.

Funding Declaration: This research received no specific grant from any funding agency.

Ethics, Consent to Participate, and Consent to Publish declarations: Not applicable

Clinical Trial: Not applicable

Authors Credit:

Sonu Choudhary (SC): Conceptualisation, Data curation, Formal analysis, Methodology, Writing Original draft, Validation; Surojit Konar (SK): Data analysis, Software, Validation; Yoheshwar Mishra (YM): Resources; Sharad Tiwari (ST): Supervision, Review & Editing, resources

References

1. Arvidson RE, Catalano JG, Christian JR, Fraeman AA, Hughes MN, Knight AL, McKinnon WB, Morris RV, Murchie SL, O'Sullivan JA, Politte DV (2026) Saponite bearing material excavated during the formation of a recent 25-m-diameter impact crater in southeastern Arabia Terra on Mars. J Geophys Res Planets 131(5):e2025JE009535. https://doi.org/10.1029/2025JE009535
2. Best L, Schwarz N, Obergh D, Teuling AJ, Van Kanten R, Willemen L (2023) Urban green spaces and variation in cooling in the humid tropics: the case of Paramaribo. Urban For Urban Green 89:128111. https://doi.org/10.1016/j.ufug.2023.128111
3. Bi Y, Liu T, Pei Y, Wang X, Du X (2025) Landscape analysis and assessment of ecosystem stability based on land use and multitemporal remote sensing: a case study of the Zhungeer open-pit coal mining area. Remote Sens 17(7):1162. https://doi.org/10.3390/rs17071162
4. Burakowski E, Tawfik A, Ouimette A, Lepine L, Novick K, Ollinger S, Zarzycki C, Bonan G (2018) The role of surface roughness, albedo, and Bowen ratio on ecosystem energy balance in the Eastern United States. Agric. https://doi.org/10.1016/j.agrformet.2017.11.030
5. Chen L, Ju L, Liu J, Jiao S, Zhang Y, Yin X, Yue C (2025) Spatiotemporal evolution and driving factors of surface temperature changes before and after ecological restoration of mines in the plateau alpine permafrost regions based on Landsat images. Earth 6(4):141. https://doi.org/10.3390/earth6040141
6. Deka J, Kalita S, Khan ML (2019) Vegetation phenological characterization of alluvial plain Shorea robusta-dominated tropical moist deciduous forest of northeast India using MODIS NDVI time series data. J Indian Soc Remote Sens 47(8):1287–1293. https://doi.org/10.1007/s12524-019-00991-x
7. Deng X, Shi Q, Zhang Q, Shi C, Yin F (2015) Impacts of land use and land cover changes on surface energy and water balance in the Heihe River Basin of China, 2000–2010. Phys Chem Earth Parts A/B/C 79:2–10. DOI:10.1016/j.pce.2015.01.002
8. Dominguez-Haydar Y, Velásquez E, Carmona J, Lavelle P, Chavez LF, Jiménez JJ (2019) Evaluation of reclamation success in an open-pit coal mine using integrated soil physical, chemical and biological quality indicators. Ecol Indic 103:182–193. https://doi.org/10.1016/j.ecolind.2019.04.015Get rights and content
9. Ekka P, Patra S, Upreti M, Kumar G, Kumar A, Saikia P (2023) Land degradation and its impacts on biodiversity and ecosystem services. In: Land and environmental management through forestry. pp 77–101. https://doi.org/10.1002/9781119910527.ch4
10. Escribano P, Palacios-Orueta A, Oyonarte C, Chabrillat S (2010) Spectral properties and sources of variability of ecosystem components in a Mediterranean semiarid environment. J Arid Environ 74(9):1041–1051. https://doi.org/10.1016/j.jaridenv.2010.02.001
11. Feldman AF, Short Gianotti DJ, Dong J, Akbar R, Crow WT, McColl KA et al (2023) Remotely sensed soil moisture can capture dynamics relevant to plant water uptake. Water Resour Res 59:e2022WR033814. https://doi.org/10.1029/2022WR033814
12. Firozjaei MK, Sedighi A, Karimi Firozjaei H, Kiavarz M, Homaee M, Jokar Arsanjani J, Makki M, Naimi B, Alavipanah SK (2021) A historical and future impact assessment of mining activities on surface biophysical characteristics change: a remote sensing-based approach. Ecol Indic 122:107264. https://doi.org/10.1016/j.ecolind.2020.107264
13. Foody GM (2020) Explaining the unsuitability of the kappa coefficient in the assessment and comparison of the accuracy of thematic maps obtained by image classification. Remote Sens Environ 239:111630. https://doi.org/10.1016/j.rse.2019.111630
14. Frazier AE, Kedron P (2017) Landscape metrics: past progress and future directions. Curr Landsc Ecol Rep 2(3):63–72. https://doi.org/10.1007/s40823-017-0026-0
15. Frouz J (2021) Soil recovery and reclamation of mined lands. In: Soils and landscape restoration. Academic Press, pp 161–191.https://doi.org/10.1016/B978-0-12-813193-0.00006-0.

16. Gottschalk P, Klumpp K, Cardinael R, Ceschia E, Diop S, Genesio L, Khalil MI, Kruijt B, Lugato E, Roujean JL, Sieber P, Osborne B (2026) Reflecting on surface albedo and climate. Clim Res 96:1–28. https://doi.org/10.3354/cr01764
17. Gong C, Wu W (2014) Comparisons of regression tree models for sub-pixel imperviousness estimation in a Gulf Coast city of Mississippi, USA. Int J Remote Sens 35(10):3722–3740
18. Haigh M, Woodruffe P, D'Aucourt M, Alun E, Wilding G, Fitzpatrick S et al (2020) Successful ecological regeneration of opencast coal mine spoils through forestation: from cradle to grove. Minerals 10(5):461. https://doi.org/10.3390/min10050461
19. Huang A, Shen R, Jia G, Xu X (2022) Reforestation enhanced landscape connectivity for thermal buffering in China. Environ Res Lett 17(1):014056. https://doi.org/10.1088/1748-9326/ac3fda
20. Hulley GC, Hughes CG, Hook SJ (2012) Quantifying uncertainties in land surface temperature and emissivity retrievals from ASTER and MODIS thermal infrared data. Journal of Geophysical Research Atmosphere 117(D23). https://doi.org/10.1029/2012JD018506
21. John R, Chen J, Kim Y, Ou-yang ZT, Xiao J, Park H et al (2016) Differentiating anthropogenic modification and precipitation-driven change on vegetation productivity on the Mongolian Plateau. Landsc Ecol 31(3):547–566. https://doi.org/10.1007/s10980-015-0261-x
22. Kandulna W, Jain MK, Chugh YP, Agarwal S (2025) Spatial variability of land surface temperature of a coal mining region using a geographically weighted regression model: a case study. Land 14(4):696. https://doi.org/10.3390/land14040696
23. Kendall MG (1975) Rank correlation methods, 4th edn. Charles Griffin, London
24. Li Y, Li H, Pan J (2024) Long-term desertification process monitoring and driving factors analysis in rare earth mining areas. Restor Ecol 32(2): e13994. https://doi.org/10.1111/rec.13994
25. Makarieva AM, Nefiodov AV, Nobre AD, Sheil D, Nobre P, Pokorný J, Hesslerová P, Li BL (2022) Vegetation impact on atmospheric moisture transport under increasing land-ocean temperature contrasts. Heliyon 8(10). https://doi.org/10.1016/j.heliyon.2022.e11173
26. Mann HB (1945) Nonparametric tests against trend. Econometrica 13(3):245–259. https://doi.org/10.2307/1907187
27. Mansingh A, Pradhan A, Gopinath JS, Rout M, Panda BP, Ekka NJ (2026) Assessing the climatic effects of landscape transformation through long-term temperature trends in an industrial region of eastern India. Environ Monit Assess 198(6):577. https://doi.org/10.1007/s10661-026-15405-y
28. Maxwell AE, Strager MP, Warner TA, Ramezan CA, Morgan AN, Pauley CE (2019) Large-area, high spatial resolution land cover mapping using random forests, GEOBIA, and NAIP orthophotography: findings and recommendations. Remote Sens 11(12):1409. https://doi.org/10.3390/rs17071162
29. McGregor G (2024) Surface atmosphere interactions and heatwaves. In: Heatwaves: causes, consequences and responses. Springer International Publishing, pp 261–304. https://doi.org/10.1007/978-3-031-69906-1_7
30. Millward AA, Torchia M, Laursen AE, Rothman LD (2014) Vegetation placement for summer-built surface temperature moderation in an urban microclimate. Environ Manage 53(6):1043–1057. https://doi.org/10.1007/s00267-014-0260-8
31. Montandon LM, Small EE (2008) The impact of soil reflectance on the quantification of the green vegetation fraction from NDVI. Remote Sens Environ 112(4):1835–1845. https://doi.org/10.1016/j.rse.2007.09.007
32. Mutti PR, Lúcio PS, Dubreuil V, Bezerra BG (2020) NDVI time series stochastic models for the forecast of vegetation dynamics over desertification hotspots. Int J Remote Sens 41(7):2759–2788. https://doi.org/10.1080/01431161.2019.1697008
33. O'Donnell MS, Whipple AL, Inman RD, Tarbox BC, Monroe AP, Robb BS, Aldridge CL (2024) Remote sensing for monitoring mine lands and recovery efforts (No. 1525). US Geological Survey. https://doi.org/10.3133/cir1525
34. Onačillová K, Gallay M, Paluba D, Péliová A, Tokarčík O, Laubertová D (2022) Combining Landsat 8 and Sentinel-2 data in Google Earth Engine to derive higher resolution land surface temperature maps in urban environment. Remote Sens 14(16):4076. https://doi.org/10.3390/rs14164076

35. Patil MB, Desai CG, Umrikar BN (2012) Image classification tool for land use/land cover analysis: a comparative study of maximum likelihood and minimum distance method. Int J Geol Earth Environ Sci 2(3):189–196
36. Pearson K (1895) Note on regression and inheritance in the case of two parents. Proc R Soc Lond 58:240–242. https://doi.org/10.1098/rspl.1895.0041
37. Pettorelli N, Laurance WF, O'Brien TG, Wegmann M, Nagendra H, Turner W (2014) Satellite remote sensing for applied ecologists: opportunities and challenges. J Appl Ecol 51(4):839–848. https://doi.org/10.1111/1365-2664.12261
38. Poole GC, Berman CH (2001) An ecological perspective on in-stream temperature: natural heat dynamics and mechanisms of human-caused thermal degradation. Environ Manage 27(6):787–802. https://doi.org/10.1007/s002670010188
39. Prasad S, Denis DM, Kumar M, Prabha S, Singh R (2025) Evaluating certain approaches for computing land surface temperature over alluvial plains of Northern India. Discov Geosci 3(1):126. https://doi.org/10.1007/s44288-025-00236-0
40. Ratul MJP, Hasher FFB, Kanetaki Z, Zhran M (2026) A comparative data-driven framework for total sediment load prediction using multi-algorithm ANN, hydro-meteorological inputs, and advanced preprocessing techniques. Water 18(10):1182. https://doi.org/10.3390/w18101182
41. Rotenberg E, Yakir D (2010) Contribution of semi-arid forests to the climate system. Science 327(5964):451–454. DOI:10.1126/science.1179998
42. Sen PK (1968) Estimates of the regression coefficient based on Kendall's tau. J Am Stat Assoc 63(324):1379–1389. https://doi.org/10.1080/01621459.1968.10480934
43. Senf C, Pflugmacher D, Heurich M, Krueger T (2017) A Bayesian hierarchical model for estimating spatial and temporal variation in vegetation phenology from Landsat time series. Remote Sens Environ 194:155–160. https://doi.org/10.1016/j.rse.2017.03.020
44. Shen B, Poulsen B, Luo X, Qin J, Thiruvenkatachari R, Duan Y (2017) Remediation and monitoring of abandoned mines. Int J Min Sci Technol 27(5):803–811. http://dx.doi.org/10.1016/j.ijmst.2017.07.026
45. Shuai Y, Tuerhanjiang L, Shao C, Gao F, Zhou Y, Xie D, Liu T, Liang J, Chu N (2020) Re-understanding of land surface albedo and related terms in satellite-based retrievals. Big Earth Data 4(1):45–67. https://doi.org/10.1080/20964471.2020.1716561
46. Snyder KA, Huntington JL, Wehan BL, Morton CG, Stringham TK (2019) Comparison of Landsat and land-based phenology camera normalized difference vegetation index (NDVI) for dominant plant communities in the Great Basin. Sensors 19(5):1139. https://doi.org/10.3390/s19051139
47. Spearman C (1904) The proof and measurement of association between two things. Am J Psychol 15(1):72–101. https://doi.org/10.2307/1412159
48. Stokes A, Douglas GB, Fourcaud T, Giadrossich F, Gillies C, Hubble T, Kim JH, Loades KW, Mao Z, McIvor IR, Mickovski SB (2014) Ecological mitigation of hillslope instability: ten key issues facing researchers and practitioners. Plant Soil 377(1):1–23. https://doi.org/10.1007/s11104-014-2044-6
49. Sun Q, Li D, Tang X, Ren Y (2025) Vegetation-specific cooling responses to compact urban development: evidence from a landscape-based analysis in Nanjing, China. Plants 14(16):2457. https://doi.org/10.3390/plants14162457
50. Szarek-Łukaszewska G (2009) Vegetation of reclaimed and spontaneously vegetated Zn-Pb mine wastes in Southern Poland. Pol J Environ Stud 18(4)
51. Tahooni A, Kakroodi AA, Kiavarz M (2023) Monitoring of land surface albedo and its impact on land surface temperature (LST) using time series of remote sensing data. Ecol Inform 75:102118. https://doi.org/10.1016/j.ecoinf.2023.102118
52. Tang L, Werner TT (2023) Global mining footprint mapped from high-resolution satellite imagery. Commun Earth Environ 4(1):134. https://doi.org/10.1038/s43247-023-00805-6
53. Theil H (1950) A rank-invariant method of linear and polynomial regression analysis. In: Henri Theil's contributions to economics and econometrics: econometric theory and methodology. Springer Netherlands, Dordrecht, pp 345–381. https://doi.org/10.1007/978-94-011-2546-8_20

54. Trilica A, Hutyra LR, Schaaf CL, Erb A, Wang JA (2017) Albedo, land cover, and daytime surface temperature variation across an urbanized landscape. Earths Future 5(11):1084–1101. https://doi.org/10.1002/2017EF000569
55. Vicentini F, Hendrychova M, Tajovský K, Pižl V, Frouz J (2020) The effect of topography on long-term spontaneous development of soil and woody cover on graded and untreated overburden. Forests 11(5):602. https://doi.org/10.3390/f11050602
56. Wang L, Yue P, Yang Y, Sha S, Hu D, Ren X, Jiang X (2025a) Land surface condition-driven emissivity variation and its impact on diurnal land surface temperature retrieval uncertainty. Remote Sens 17(14):2353. https://doi.org/10.3390/rs17142353
57. Wang S, Zhang S, Zhou Y, Zhao X, Li R, Lin X, Luo M, Yang L, Zhang Q, Lv S, Yang Y (2025b) Vegetation disturbance and recovery assessment through the synergistic effects of albedo and vegetation index: evidence from China's arid regions. Ecol Indic 178:113856. https://doi.org/10.1016/j.ecolind.2025.113856
58. Waseem S, Khayyam U (2019) Loss of vegetative cover and increased land surface temperature: a case study of Islamabad, Pakistan. J Clean Prod 234:972–983. https://doi.org/10.1016/j.jclepro.2019.06.228
59. Weng Q, Lu D, Schubring J (2004) Estimation of land surface temperature–vegetation abundance relationship for urban heat island studies. Remote Sens Environ 89(4):467–483. https://doi.org/10.1016/j.rse.2003.11.005
60. Wu H, Huang B, Zheng Z, Ma Z, Zeng Y (2022) Spatial heterogeneity and temporal variation in urban surface albedo detected by high-resolution satellite data. Remote Sens 14(23):6166. https://doi.org/10.3390/rs14236166
61. Yang J, Liu Q, Luo Y, Yin Y, Lu X (2025) Rapid dynamics of paraglacial vegetation under temperate deglaciating environments in Mt. Gongga, southeastern Tibetan Plateau. J Geogr Sci 35(9):1979–1. https://doi.org/10.1007/s11442-025-2399-z
62. Yengoh GT, Dent D, Olsson L, Tengberg AE, Tucker III CJ (2015) Use of the Normalized Difference Vegetation Index (NDVI) to assess land degradation at multiple scales: current status, future trends, and practical considerations. DOI:10.1007/978-3-319-24112-8
63. Zhang C, Su Y, Liu L, Wu J, Huang G, Li X et al (2023) Seasonal and long-term dynamics in forest microclimate effects: global pattern and mechanism. npj Clim Atmos Sci 6(1):116. https://doi.org/10.1038/s41612-023-00442-y
64. Zhang X, Jiao Z, Zhao C, Qu Y, Liu Q, Zhang H et al (2022) Review of land surface albedo: variance characteristics, climate effect and management strategy. Remote Sens 14(6):1382. https://doi.org/10.3390/rs14061382
65. Zhou X, Wang YC (2010) Dynamics of land surface temperature in response to land-use/cover change. Geogr Res 49(1):23–36. DOI:10.1111/j.1745-5871.2010.00686.x
66. Zine H, Hakkou R, Papazoglou EG, Elmansour A, Abrar F, Benzaazoua M (2024) Revegetation and ecosystem reclamation of post-mined land: toward sustainable mining. Int J Environ Sci Technol 21(15):9775–9798. https://doi.org/10.1007/s13762-024-05697-3

Supplementary Files

This is a list of supplementary files associated with this preprint. Click to download.

- Supplementaryfile.docx